Scripta Materialia 140 (2017) 31–34

Contents lists available at ScienceDirect

Scripta Materialia

journal homepage: www.elsevier.com/locate/scriptamat

Regular article

Significant strengthening of nanocrystalline Ni sub-micron pillar by cyclic loading in elastic regime

Jung-A Lee [a], Dong-Hyun Lee [a], Moo-Young Seok [b], In-Chul Choi [c], Heung Nam Han [d], Ting Y. Tsui [e,*], Upadrasta Ramamurty [f], Jae-il Jang [a,*]

[a] Division of Materials Science and Engineering, Hanyang University, Seoul 04763, Republic of Korea
[b] Max-Planck-Institut für Eisenforschung GmbH, Max-Planck-Straße 1, Düsseldorf 40237, Germany
[c] Institute for Applied Materials, Karlsruhe Institute of Technology, Karlsruhe 76021, Germany
[d] Department of Materials Science and Engineering, Seoul National University, Seoul 08826, Republic of Korea
[e] Department of Mechanical Engineering, University of Waterloo, 200 University Avenue West, Waterloo, ON N21 3G1, Canada
[f] Department of Materials Engineering, Indian Institute of Science, Bangalore 560012, India

ARTICLE INFO

Article history:
Received 20 June 2017
Received in revised form 29 June 2017
Accepted 5 July 2017
Available online 8 July 2017

Keywords:
Nanocrystalline metals
Micro-compression test
Cyclic loading

ABSTRACT

The influence of cyclic load, with the maximum stress well within the elastic regime, on the strength of nanocrystalline (nc) nickel was investigated through quasi-static compression experiments on cyclic-loaded sub-μm-sized pillars, fabricated through electron beam lithography and electroplating. Results show that prior-cycling enhances both yield and flow strengths of nc Ni without significant loss in plasticity. Changes in strain-rate sensitivity and activation volume for deformation upon cycling were measured and utilized to discuss possible mechanisms responsible for the observed strengthening.

The mechanical behavior of nanocrystalline (nc) metals with small volume such as nano-/micro-pillars is an active research topic, especially because there can be both extrinsic and intrinsic size effects (i.e., influences of pillar diameter, D and grain size, d) [1–8]. While extensive research, which was performed on these nc pillars hitherto, has uncovered plethora of interesting and exciting deformation behavior that arise as d is reduced to nm scale, most of it was performed under static or quasi-static loading conditions. However, the effect of cycling loading on the mechanical behavior (which is essential for ensuring reliability in structural applications where load fluctuations are common) of nc pillars remains unexplored although results of cyclic loading tests were reported for bulk samples of nc metals [9–12] or micro-pillars of single crystal and metallic glass [13–16].

Fatigue in crystalline metals is primarily a consequence of the kinematic irreversibility of slip [17]. Since nc metals offer more possibilities for such irreversibility to occur, by virtue of the large grain boundary (GB) area, their susceptibility for fatigue-induced property changes can be expected to be relatively more in comparison to their microcrystalline counterparts. Indeed, Moser et al. [9], who studied the cyclic plasticity of electrodeposited nc Ni ($d = 40$ nm), reported that cyclic loading leads to considerable hardening of the metal and attributed it to the dislocation source exhaustion at GBs. Molecular dynamics simulations by Rupert and Schuh [18] reported some evidence for strengthening in nc Ni ($d = 3$, 4, 5 and 10 nm). Only two cycles can cause grain rotation, which leads to enhanced boundary coherency, i.e., formation of GBs with low coincident site lattice values (Σ) such as $\Sigma 3$ (twin boundary) that have lower energies and less stress concentration, which can lower the stress required for onset of plasticity otherwise.

Notably, Moser et al.'s experiments [9] were conducted wherein the maximum nominal stress of the tension-tension cyclic loading, S_{max}, exceeds the tensile yield strength, σ_y, of the nc Ni (see Fig. 1 of their paper). However, S_{max} does not need to necessarily exceed σ_y for kinematic irreversibility to set in; the fact that the endurance limit of most metals can be as low as 0.35 to 0.5 times σ_y is a testament for this. Further, and already mentioned, nc metals can offer more avenues for fatigue induced irreversible microstructural changes. Therefore, it is reasonable to anticipate that cyclic loading, even when S_{max} is well below σ_y, i.e., the deformation during cycling being nominally elastic, can significantly alter the mechanical behavior of the metals.

We critically examine this possibility by conducting experiments on sub-μm-sized pillars of nc Ni that were prepared through high-throughput electron beam lithography and electroplating process [19]. A series of cyclic and subsequent monotonic micro-compression tests reveal that both yield strength and flow stress significantly increase because of prior-cyclic loading. Mechanistic origins for the observed hardening are discussed in terms of strain-rate sensitivity, and activation volume for deformation, etc.

* Corresponding authors.
E-mail addresses: tttsui@uwaterloo.ca (T.Y. Tsui), jijang@hanyang.ac.kr (J. Jang).

http://dx.doi.org/10.1016/j.scriptamat.2017.07.001
1359-6462/

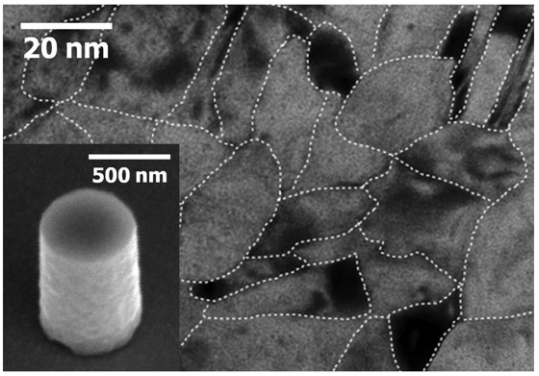

Fig. 1. Representative TEM image showing the grain structure of as-fabricated nc Ni pillars (with inset of SEM image for pillar morphology).

The sub-μm-sized nc Ni pillars examined in this study were prepared through electron beam lithography and electroplating techniques [19]. Thin ~20 nm Ti (adhesion layer) and ~40 nm Au (conductive seed layer) were sequentially deposited on silicon substrates, that were subsequently spin coated by polymethylmethacrylate (PMMA) resist. Arrays of ~580 nm diameter via-holes were patterned on the resist using electron beam lithography and then filled nc Ni by electroplating (with the exposed Au layer acting as the cathode and a commercial grade pure Ni as the anode). The Ni plating solution was made of Ni (II) sulfate hexahydrate (99%, Sigma Aldrich, St. Louis, MO), Ni (II) chloride (98%, Sigma Aldrich), boric acid (BX0865, EMD Millipore), and organic additive saccharin (98%, Sigma Aldrich). After plating, the PMMA resist was dissolved in a bath of acetone, to obtain nc Ni pillars. This fabrication technique has many advantages over that which used focused ion beam (FIB) milling. For example, hundreds of highly uniform pillars can be produced at the same time (which saves time and cost, and allows for statistically significant amount of experimentation and data analysis [8,20]). Importantly, one does not need to worry at all about the usual concern of surface damage that arises when FIB milled micropillars are used. The morphologies and microstructures of pillars were observed using scanning and transmission electron microscopies (SEM: JSM-6330F, and TEM: JEM-2010F, both equipment from JEOL Ltd., Tokyo, Japan), respectively.

Cyclic and subsequent quasi-static compression tests of the pillars were conducted using Nanoindenter XP (formerly MTS; now Keysight, Santa Rosa, CA) equipped with a FIB-milled cylindrical diamond punch. Compression-compression cyclic loading was performed up to a predetermined number of cycles, N (= 10, 20, 100 and 200), with S_{max} of 1000 MPa (that is below σ_y ~ 1.6–1.8 GPa) with a stress ratio R ($= S_{min} / S_{max}$ where S_{min} is the minimum stress) of 0.1 at a frequency λ of 0.5 Hz. In order to directly observe the possible change in pillar morphology during cyclic loading, in-situ compression tests were conducted by using a PI 85 picoindenter (Hysitron Inc., Mineapolis, MN) set inside a Quanta 250 FEG scanning electron microscope (FEI Inc., Hillsboro, OR). Quasi-static compression tests of both as-fabricated and cyclic-loaded pillars were performed under different nominal strain rates, $\dot{\varepsilon}$, of 0.0005, 0.002, and 0.005 s^{-1}. More than 10 measurements were conducted for each condition so as to obtain data with fidelity. Thermal drift was maintained below 0.03 nm/s in all the experiments.

A representative micrograph of the pillar was displayed in the inset of Fig. 1. The top surfaces of the pillars are flat while the side-surfaces are almost taper-free. The nominal outer diameter, D, of the pillars is ~580 nm and the height-to-diameter aspect ratio is ~1.5. A TEM image of the representative microstructure of as-fabricated pillars is displayed in Fig. 1. The average grain size, d, was determined as ~12 ± 3 nm, which was measured using multiple TEM micrographs taken at various locations of each pillar.

The pillars were subjected to compression-compression cyclic loading with sawtooth shape waveform (Fig. 2a). From the applied load, P, and displacement, h, responses recorded, engineering stress, S ($= P / A_0$, where A_0 is the initial cross-sectional area of pillar) vs. engineering strain, e ($= h / L_0$ where L_0 is the initial pillar height) were obtained. An example of S–e response is shown in Fig. 2b (for $N = 200$, which is the maximum N applied in this study). Note that $S_{max} \ll \sigma_y$ (~1.6–1.8 GPa), i.e., deformation during the entire cycling is well within the elastic limit. For clarity, only the data for every 20 cycles are shown in Fig. 2b. Hysteresis was observed during early cycles. The width of the loops reaches a steady state at N of ~30. The area of the hysteresis loop, $\Delta\Gamma$, a measure of the strain energy dissipated during that cycle, is evaluated and plotted as a function of N in the inset of Fig. 2b. It shows that $\Delta\Gamma$ decreases markedly within the first 20 cycles or so, before becoming negligible. To directly visualize cyclic deformation (if any), in-situ cyclic tests were performed under identical experimental conditions ($S_{max} = 1$ GPa, $R = 0.1$, $\lambda = 0.5$ Hz, and $N = 200$) while the pillars were imaged (see the corresponding movie in Supplementary material). In Fig. 2c, the obtained S–e curve and representative SEM images of a pillar before and after in-situ cyclic tests are displayed. The geometry of the pillar remains apparently unchanged, indicating the absence of noticeable plastic deformation or localized failure until $N = 200$.

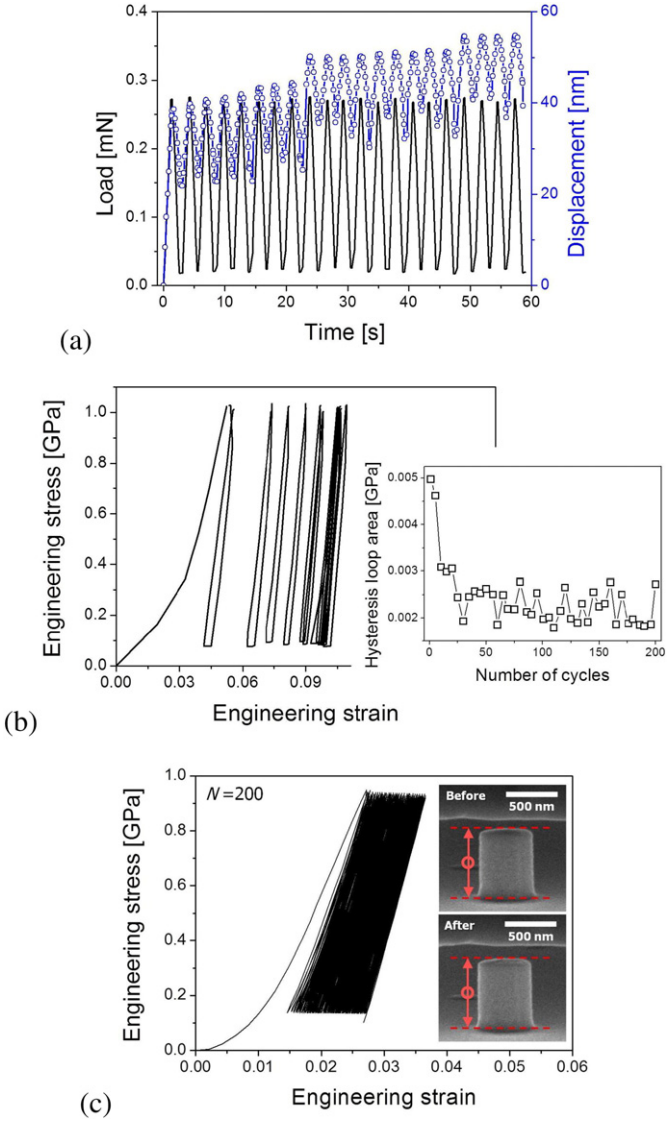

Fig. 2. Results of cyclic tests: (a) load vs. time and displacement vs. time obtained during cyclic loading; (b) converted engineering stress-strain responses with inset of hysteresis loop area as a function of N; (c) the curve from in-situ SEM experiments and the SEM images taken before and after cyclic loading.

Post-cyclic loading, the pillars were subjected to quasi-static compression tests. Representative true stress (σ) vs. true strain (ε) responses, which were made assuming volume conservation (i.e., $A_0L_0 = A_pL_p$ where A and L are cross-sectional area and height of pillar, respectively, while subscripts "0" and "p" indicate "initial" and "during plastic deformation," respectively), are displayed in Fig. 3a. While no apparent change in the elastic responses of the pillars due to prior-cyclic loading could be detected, both yield and plastic flow stresses were observed to increase with N. Variations σ_y (obtained by a strain offset of 1% [8]), and flow stress, σ_f (estimated at remnant plastic strain ε_p, which is the amount ε that remains after unloading [8], of 10%) with N are displayed in Fig. 3b. Here, $N = 0$ refers to as-fabricated condition. Both σ_y and σ_f increase significantly with N, with the majority of the strengthening occurring within the first 20 cycles or so. The latter observation is consistent with trends seen in $\Delta\Gamma$.

To investigate the possible mechanisms responsible for the enhanced strength due to cycling, we first studied the strain-rate sensitivity (SRS), m, which not only indicates to the dominant deformation mechanism, but also provides indirect information about the plasticity as a higher m often corresponds to a larger ability to accommodate plastic deformation. The value of m can be determined at a given ε and temperature, T, from the relation: $m = (\partial \ln\sigma_f/\partial \ln\dot{\varepsilon})_{\varepsilon,T}$. We have evaluated it for $N = 0$, 20, and 200, from the slopes of the double logarithmic plots of σ_f versus $\dot{\varepsilon}$, as displayed in Fig. 4. In the as-fabricated state, m is ~0.037, which decreases to ~0.030 upon subjecting the pillars to 20 cycles; it further reduces to ~0.017 for $N = 200$. While all these are within the range of m reported for bulk nc metals that have fcc crystal structure (e.g., m ~ 0.01–0.03 [21–23]), the observed trend in Fig. 4 suggests that cyclic loading definitely reduces the SRS, which may reduce the ductility but not in any substantial manner, even though it leads remarkable strengthening.

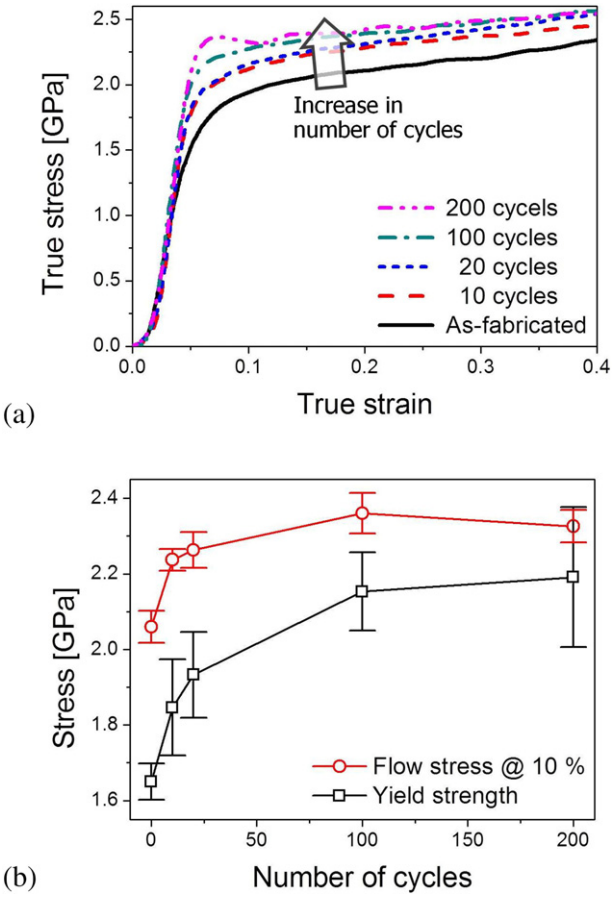

Fig. 3. Results of monotonic compression tests: (a) true stress-true strain curves and (b) changes in yield strength and flow stress as a function of N.

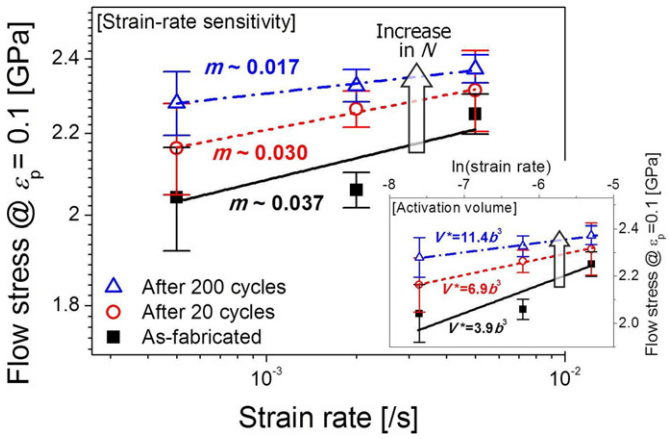

Fig. 4. Estimation of strain-rate sensitivity and activation volume (in inset) of as-fabricated and cyclic-loaded pillars.

Strengthening by cyclic loading has been reported for coarse-grained metals with susceptibility for cross-slip in which dislocations may interact with each other and form locks, leading to hardening [17]. Given that the experiments of the current study were performed on sub-μm-sized pillars (D = ~580 nm), the additional possibility of dislocation migration to the free surfaces during cycling and eventual annihilation there, leading to far fewer dislocations in the fatigued materials and hence higher stress required for subsequent plastic deformation, needs consideration. Recently, Wang et al. [14] and Cui et al. [24] reported such strengthening of single crystal Al pillars during low-amplitude cyclic loading. While we cannot rule out such possibility in the present context (as discussed later), such an effect might not be a major contributor to the observed strengthening since only a small fraction of the grains are exposed to the free surface, as d is much smaller than D.

To gain further insights into the plastic deformation mechanism, activation volume for plastic deformation, V^* was estimated by using the relation: $V^* = \sqrt{3}kT(\partial \ln\dot{\varepsilon}/\partial\sigma_f)$, where k is the Boltzmann's constant. Note that the value of V^* varies by orders of magnitude for different rate-limiting processes [25] with typical values of V^* in the ranges of ~1–10b^3 for diffusion either through the crystalline lattice and along the GB [26,27], ~10b^3 for GB sliding [28], and ~100–1000b^3 for dislocation glide [26]. The value of V^* was determined from the slope of the linear fit of logarithmic $\dot{\varepsilon}$ versus linear σ_f (see the inset of Fig. 4). While V^* for as-fabricated ($N = 0$) nc Ni is ~3.9b^3, it increases to ~6.9b^3 for N = 20 and ~11.4b^3 for $N = 200$ (where b is Burgers vector and 0.249 nm for Ni) specimens. While these results do indicate to a systematic increase V^*, we can conclude that the dominant deformation mechanism does not get affected in any significant manner by the prior-cyclic loading as V^* does not change by orders of magnitude. Note that grain refinement to nanometer scale leads to a decrease in V^* due to the increased role of GBs [29,30]. Similarly, it was also reported that the values of V^* are reduced in small-sized sample [31,32]. Thus, we conclude that the predominant deformation mechanism of our sample is GB-mediated plasticity, which can be additionally enhanced by the free surface. On this basis, we identify three possible mechanisms for the cyclic-loading-induced strengthening.

First, we consider the role of GBs in the plastic flow of nc metals and the possibility of the exhaustion of dislocation sources at GBs during cycling causing strengthening, as suggested by Moser et al. [9]. They observed that such exhaustion mainly occurs in the early stages of cycling where strain amplitude and hysteresis loop area rapidly decrease, similar to that seen in the present study. Following this, the significant decrease in hysteresis loop area in first 10–20 cycles (as shown in inset of Fig. 2b) observed in the present study is related to exhaustion of dislocation sources at GBs. In this context, it is natural to wonder if such a mechanism can be invoked especially since $S_{max} \ll \sigma_y$. The macroscopic yield

of metal, for which σ_y is the measure of, corresponds to a large number of dislocations being active. Dislocation activity does indeed take place even when the applied stresses are well below σ_y. For example, a straight segment of dislocation that is pinned at two ends can bow through the grain during stressing, purely from elastic stress considerations. Since the d is extremely small in nc metals, such a bowing dislocation can get absorbed at the GBs, causing kinematic irreversibility. Indeed, the large fraction of GBs in nc metals plays a critical role in plastic flow (including diffusion-based activities and dislocation emission/absorption) [33–35].

Research on the state of GBs is one of the important topics in the nc field and the GB relaxation has been reported through low-temperature annealing [36–39], which is qualitatively similar to cyclic-loading-induced strengthening. Rupert et al. [37] estimated the activation energy for GB relaxation in nc Ni—W (with d ~ 12 nm) as ~50 kJ/mol which is lower than that for GB diffusion (~115 kJ/mol [27]). In addition, it is noteworthy that such boundary relaxation can promote shear localization [36,37], indicating that no significant ductility loss (evidenced by SRS in Fig.4) may be related to lower GB energy.

Another possibility for the observed strengthening can be associated with free surface. Although free surfaces take small portion vis-a-vis GBs, they can still play a minor and yet important role in plastic deformation in small-volume structures. It was reported in literature [7,40–42] that a smaller pillar with a higher surface-to-volume ratio exhibited more pronounced room-temperature creep deformation under low stress in elastic regime, which is rationalized by diffusion-assisted process along free surface. In this context, one can expect that surface diffusion assisted deformation occurs during cyclic loading even in the elastic regime. Molecular dynamics study by Fan et al. [43] suggested surface reconstruction by cyclic loading due to energy gradient at surface step and/or surface diffusion. Therefore, by applying cyclic loading surface configuration can be changed into more stable state, reducing local stress concentrations at the surface defects and making further plastic deformation more difficult.

The third and final possibility is the alteration of the residual lattice stress/strain due to cyclic loading. If there are some residual stresses in the lattices of the nc pillars, arising out of the processing, the strength of the pillars can change when such stresses are relieved due to cycling. In this regard, Cheng et al. [10] investigated cyclic deformation of nc Ni (d ~ 20 nm) and ultrafine-grained (ufg) Ni (d ~ 100 and 1000 nm) under tension-tension loads. While cyclic loading altered residual lattice strains in ufg Ni, nc Ni did not show any noticeable change in residual lattice strain, which is almost zero. However, their experimental conditions [10] are significantly different from those used in the current study: d is smaller and applied stress is much lower (below σ_y). Thus, this possibility cannot be entirely excluded, although it is still very low since the pillars of this investigation was processed using lithographic techniques, which do not allow for residual stress build-up.

In summary, we have investigated the influence of prior-cyclic loading, with the maximum stress of the cycle being well within the elastic regime, on the strength of sub-μm-sized nc Ni pillars through cyclic and subsequent monotonic compression tests. The experimental results show that cycling loading causes significant strengthening, especially within the first ~20 cycles. Such strengthening may be caused by GB relaxation, surface reconfiguration, and residual strain change, all of which can lead to enhanced resistance to plastic deformation.

The work was supported by the National Research Foundation of Korea (NRF) grant funded by the Korea government (MSIP) (No. 2015R1A5A1037627 and No. 2017R1A2B4012255). The authors wish to thank Brandon B. Seo for his valuable support with pillar fabrication.

Appendix A. Supplementary data

Supplementary data to this article can be found online at http://dx.doi.org/10.1016/j.scriptamat.2017.07.001.

References

[1] J.R. Greer, J.T.M. De Hosson, Prog. Mater. Sci. 56 (2011) 654–724.
[2] J.R. Greer, D. Jang, X.W. Gu, JOM 64 (2012) 1241–1252.
[3] D. Jang, J.R. Greer, Scr. Mater. 64 (2011) 77–80.
[4] X.W. Gu, C.N. Loynachan, Z. Wu, Y.-W. Zhang, D.J. Srolovitz, J.R. Greer, Nano Lett. 12 (2012) 6385–6392.
[5] B.B. Seo, Z. Jahed, M.J. Burek, T.Y. Tsui, Mater. Sci. Eng. A 596 (2014) 275–284.
[6] N.L. Okamoto, D. Kashioka, T. Hirato, H. Inui, Int. J. Plast. 56 (2014) 173–183.
[7] J.-A. Lee, B.B. Seo, I.-C. Choi, M.-Y. Seok, Y. Zhao, Z. Jahed, U. Ramamurty, T.Y. Tsui, J.-I. Jang, Scr. Mater. 112 (2016) 79–82.
[8] J.-A. Lee, M.-Y. Seok, Y. Zhao, I.C. Choi, D.H. Lee, B.B. Seo, U. Ramamurty, T.Y. Tsui, J.-I. Jang, Acta Mater. 127 (2017) 332–340.
[9] B. Moser, T. Hanlon, K.S. Kumar, S. Suresh, Scr. Mater. 54 (2006) 1151–1155.
[10] S. Cheng, J. Xie, A.D. Stoica, X.-L. Wang, J.A. Horton, D.W. Brown, H. Choo, P.K. Liaw, Acta Mater. 57 (2009) 1272–1280.
[11] X.H. An, Q.Y. Lin, S.D. Wu, Z.F. Zhang, Scr. Mater. 68 (2013) 988–991.
[12] J. Hu, J. Zhang, Z. Jiang, X. Ding, Y. Zhang, S. Han, J. Sun, J. Lian, Mater. Sci. Eng. A 651 (2016) 999–1009.
[13] R.J. Milne, A.J. Lockwood, B.J. Inkson, J. Phys. Conf. Ser. 241 (2010), 012059.
[14] Z.-J. Wang, Q.-J. Li, Y.-N. Cui, Z.-L. Liu, E. Ma, J. Li, J. Sun, Z. Zhuang, M. Dao, Z.-W. Shan, S. Suresh, Proc. Natl. Acad. Sci. 112 (2015) 13502–13507.
[15] M. Schamel, J.M. Wheeler, C. Niederberger, J. Michler, A. Sologubenko, R. Spolenak, Philos. Mag. 96 (2016) 3479–3501.
[16] D. Jang, R. Maaß, G. Wang, P.K. Liaw, J.R. Greer, Scr. Mater. 68 (2013) 773–776.
[17] S. Suresh, Fatigue of Materials, Second ed. Cambridge University Press, Cambridge, 1998.
[18] T.J. Rupert, C.A. Schuh, Philos. Mag. Lett. 92 (2012) 20–28.
[19] M.J. Burek, J.R. Greer, Nano Lett. 10 (2010) 69–76.
[20] Y. Gao, H. Bei, Prog. Mater. Sci. 82 (2016) 118–150.
[21] S. Cheng, E. Ma, Y.M. Wang, L.J. Kecskes, K.M. Youssef, C.C. Koch, U.P. Trociewitz, K. Han, Acta Mater. 53 (2005) 1521–1533.
[22] F. Dalla Torre, H. Van Swygenhoven, M. Victoria, Acta Mater. 50 (2002) 3957–3970.
[23] Y.M. Wang, E. Ma, Appl. Phys. Lett. 85 (2004) 2750–2752.
[24] Y.-n. Cui, Z.-l. Liu, Z.-j. Wang, Z. Zhuang, J. Mech. Phys. Solids 89 (2016) 1–15.
[25] T. Zhu, J. Li, A. Samanta, H.-G. Kim, S. Suresh, Proc. Natl. Acad. Sci. U. S. A. 104 (2007) 3031–3036.
[26] H. Conrad, Mater. Sci. Eng. A 341 (2003) 216–228.
[27] H.J. Frost, M.F. Ashby, Deformation-Mechanism Maps, Pergamon Press, Oxford, 1982.
[28] H. Conrad, Nanotechnology 18 (2007) 325701.
[29] Y.M. Wang, A.V. Hamza, E. Ma, Acta Mater. 54 (2006) 2715–2726.
[30] E. Ma, Science 350 (2004) 623–624.
[31] T. Zhu, J. Li, Prog. Mater. Sci. 55 (2010) 710–757.
[32] C. Peng, Y. Zhong, Y. Lu, S. Narayanan, T. Zhu, J. Lou, Appl. Phys. Lett. 102 (2013), 083102.
[33] K.S. Kumar, S. Suresh, H. Van Swygenhoven, Acta Mater. 51 (2003) 5743–5774.
[34] M.A. Meyers, A. Mishra, D.J. Benson, Prog. Mater. Sci. 51 (2006) 427–556.
[35] M. Dao, L. Lu, R.J. Asaro, J.T.M. De Hosson, E. Ma, Acta Mater. 55 (2007) 4041–4065.
[36] T.J. Rupert, J. Appl. Phys. 114 (2013), 033527. .
[37] T.J. Rupert, J.R. Trelewicz, C.A. Schuh, J. Mater. Res. 27 (2012) 1285–1294.
[38] D. Jang, M. Atzmon, J. Appl. Phys. 99 (2006), 083504. .
[39] A.J. Detor, C.A. Schuh, J. Mater. Res. 22 (2007) 3233–3248.
[40] B.-G. Yoo, J.-Y. Kim, Y.-J. Kim, I.-C. Choi, S. Shim, T.Y. Tsui, H. Bei, U. Ramamurty, J.-I. Jang, Int. J. Plast. 37 (2012) 108–118.
[41] I.-C. Choi, Y.-J. Kim, M.-Y. Seok, B.-G. Yoo, J.-Y. Kim, Y.M. Wang, J.-I. Jang, Int. J. Plast. 41 (2013) 53–64.
[42] Y.-J. Kim, W.W. Lee, I.-C. Choi, B.-G. Yoo, S.M. Han, H.-G. Park, W.I. Park, J.-I. Jang, Acta Mater. 61 (2013) 7180–7188.
[43] Z. Fan, O.H. Duparc, M. Sauzay, Acta Mater. 102 (2016) 149–161.